Journal of
Marine Science and Engineering

MDPI

Article

Methodology Based on Photogrammetry for Testing Ship-Block Resistance in Traditional Towing Tanks: Observations and Benchmark Data

José Enrique Gutiérrez-Romero [1,*], Samuel Ruiz-Capel [1], Jerónimo Esteve-Pérez [1], Blas Zamora-Parra [2] and Juan Pedro Luna-Abad [2]

[1] Naval Architecture Technology Department, Universidad Politécnica de Cartagena, 30202 Cartagena, Spain; samuel.rcapel@edu.upct.es (S.R.-C.); jeronimo.esteve@upct.es (J.E.-P.)
[2] Fluid and Thermal Department, Universidad Politécnica de Cartagena, 30202 Cartagena, Spain; blas.zamora@upct.es (B.Z.-P.); jp.lunaabad@upct.es (J.P.L.-A.)
* Correspondence: jose.gutierrez@upct.es

Abstract: The real resistance that a ship must face when it is navigating in ice floes is the key factor for knowing the necessary power and the required engine size. The aim of this work is to provide valuable data to help other research in which numerical frameworks will be developed to study ship navigation in broken ice. In this work, we used paraffin wax as an alternative to obtain affordable solutions, avoiding the high cost of ice tests. The experiments were carried out in a traditional basin facility and they consisted of towing tank tests with a ship model using different concentrations of blocks simulated by the use of paraffin wax. Photogrammetry was used as technique to determine the initial position of the ice blocks, which is important as starting data in the current development of numerical simulation code for studying the features of ship resistance in drift ice. These data are available for some ice concentrations in attached files. In addition, a procedure for testing in traditional towing facilities is presented and discussed. The results of the resistance obtained in the experiments in the presence of simulated floes are presented for three concentrations and three model speeds. Some findings may be applicable to ice sailing, under given circumstances.

Keywords: paraffin wax blocks; ship resistance; photogrammetry; uncertainties; model-scale test; benchmark data

Citation: Gutiérrez-Romero, J.E.; Ruiz-Capel, S.; Esteve-Pérez, J.; Zamora-Parra, B.; Luna-Abad, J.P. Methodology Based on Photogrammetry for Testing Ship-Block Resistance in Traditional Towing Tanks: Observations and Benchmark Data. *J. Mar. Sci. Eng.* **2022**, *10*, 246. https://doi.org/10.3390/jmse10020246

Academic Editors: Md Jahir Rizvi and Apostolos Papanikolaou

Received: 5 January 2022
Accepted: 7 February 2022
Published: 11 February 2022

1. Introduction

Year after year, due to the effects of human industrial activities that pump Green House Gases (GHG) emissions into the atmosphere, the average temperature of the planet is rapidly increasing. It is well known that this increase in global temperature is affecting all areas of Earth differently in the form of climate change. Over the last two decades, Arctic surface air temperature has increased at more than double the global average and studies point to a trend towards higher temperatures in the Arctic [1].

As the temperature increases, sea ice melts and ice cover recedes. This allows more energy to be absorbed from the radiation of the sun, generating a loop of ice melting. These declining sea ice trends have made it possible for ships to navigate Arctic waters for longer durations in summer. Shipping companies and cargo vessels operators are considering new market opportunities in Arctic waters related to natural resources exploitation, new destinations for maritime traffic, and new routes for transit [2]. The shipping through the Arctic Ocean presents a high potential for time and cost savings compared to traditional shipping routes connecting Europe, Asia, and America (see Figure 1).

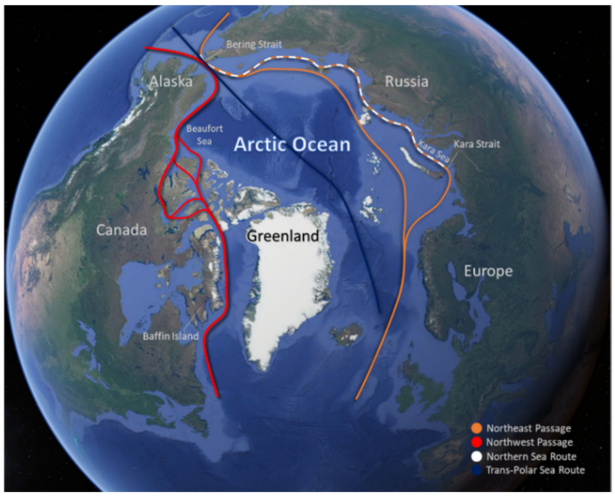

Figure 1. Arctic routes for shipping: Northeast Passage (orange), Northwest Passage (red), Northern Sea Route (white broken line), and Trans-Polar Sea Route (dark blue). Adapted from Google Maps.

As long as these routes are used, the actual presence of sea ice cannot be underestimated. The presence of ice (in several forms) is considered an additional hydrodynamic resistance with respect to the open water resistance for ships navigating in ice. This added resistance means extra engine capacity for optimal open water engines, which entails extra costs, additional lightship weight, and higher emissions. It is clear that too small engine is not sufficient to propel ships in ice conditions encountered during voyages. An engine larger than required in standard conditions results in having to move more weight than needed, higher initial and operational costs, and more pollution. Making good predictions in the design stages is crucial to avoiding those undesirable consequences. Therefore, many methods to study different kind of ice resistance have been developed since researchers have focused their interests on ship–ice interaction. In the beginning, researchers used materials to simulate ice such as wood, polyethylene, polypropylene, and paraffin wax. With the advent of ice model facilities, it became possible to create ice from frozen water appropriately mixed with additives. Different ice modeling facilities use refrigerated ice (columnar or granular ice), EG/AD/S (diluted aqueous solution of ethylene glycol (EG), aliphatic detergent (AD) and sugar (S)) [3], and urea. These are the most used techniques in ice tanks worldwide [4].

Early studies were focused on the study of ship resistance in level ice, which is assumed to be the highest resistance a ship must face in ice-covered waters. Lindqvist [5] developed one of the most used empirical methods to predict the resistance of ships in level ice. From the results of full-scale tests, he considered the superposition principle and divided the total resistance into open water resistance and ice resistance. Then, he separated the ice resistance into crushing, bending, and submersion components. Riska et al. [6] modified the equations of Lindqvist to provide a new formulation of ship resistance in level ice.

Initially, researchers paid attention to motion resistance of structures in floating ice related to offshore activities. However, some studies have been published about ship navigation in broken ice, mainly conditions for pack and brash ice, since it is important to determine this resistance due to the many times ships encounter these ice formations during a voyage. Sandkvist [7] studied the features of brash ice in the harbor of Luleå. He studied the data collected by the icebreaker "Valkyria" when passing repeatedly in an ice-covered channel, in order to create a growth and distribution model for brash ice during winter. Kitazawa and Ettema [8] also studied ship resistance in brash ice. They conducted experimental tests of a tanker model ship in a simulated brash ice channel in a model-ice towing tank to investigate the forces encountered by commercial ships transiting brash ice channels. From the results, these authors concluded that the resistance to hull motion through brash ice was the sum of bow resistance due to friction and the accumulation

of brash ice due to the submergence of brash ice beneath the hull and the momentum exchange between hull and brash ice, as well as parallel-part resistance due to friction, stern thrust due to ascension of brash ice at the stern of the hull, and open water resistance.

Aboulazm [9] studied ship-ice interaction in fragmented ice and developed a method to numerically calculate ship resistance in broken ice with energy losses due to continuous and repeated impacts with ice fragments. The prediction was good for moderate speeds with relatively small concentration of small ice fragments.

Riska et al. [6] also proposed a method to determine ship-ice resistance in brash ice channels. This ice resistance was divided into brash ice resistance, which is treated using soil mechanics and based on equations of Englund [10] and Wilhelmson [11], and an upper consolidated layer, which is considered as level ice and solved with the equations based on Lindqvist's formulas [5].

Molyneux [12] describes the model tests of the ship MV Arctic and an icebreaker, together with full-scale trials conducted by the Canadian Coast Guard, to gather information about ship performance in Labrador ice conditions. He found a good correlation between the icebreaker trials and the model tests, and found that the resistance force increased if there was pressure in the pack ice. More recently, Grochowalski and Hermanski [13] presented a study of a ship model in pack ice conditions. They studied different hull forms to assess the best to navigate in pack ice, and gave a formula for predicting pack ice resistance related to level ice resistance.

1.1. Numerical Modellings

The introduction of numerical methods has allowed researchers to simulate ice conditions and study ship-ice interaction without the need to conduct expensive experimental tests or full-scale trials. Many researchers have started to develop their own numerical tools, validating them against experimental results. Over the last few years, climate changes have made broken ice conditions more frequent in nature, resulting in an increase in the studies for such conditions. In addition, the high costs of conducting experimental tests in an ice model basin lead researchers towards the experimentation with artificial ice made of materials that do not need refrigeration, such as polypropylene plates and paraffin wax.

Konno et al. [14,15] developed a numerical solver for estimating ship resistance in brash ice channel and compared it with existing data from model tests. In order to simulate the ice motion, they considered the solids (ice pieces) and the ship as rigid bodies. Kim et al. [16,17] made tests at the Pusan National University towing tank with synthetic ice made of right triangle shaped fragments of semi-refined paraffin wax and compared the results with those obtained with a test using EG/AD/S and numerical methods. Later, these authors carried out experiments with model ships to investigate the effect of waterline angles of a ship on the resistance in pack ice conditions. They used their previous validated numerical method based on the Fluid Structure Interaction (FSI) method in the commercial Finite Elements Method (FEM) software LS-DYNA to compare results by studying three different waterline angles at three concentrations for experimental tests with synthetic ice, as well as numerical simulations. Van Der Werff et al. [18] used artificial ice in the Concept Basin of MARIN made out of rigid polypropylene (PP) particles. These authors made a 'fishbone' pre-sawn ice channel surrounded by large PP plates, similar to ice conditions in refrigerated model test facilities. Zhang et al. [19] developed a tool to obtain ice positions through image processing by using the Gradient Vector Flow (GVF) snake method and distance transform. This method allows the separation of the contours of ice pieces that initially seem to be connected. Jeong et al. [20] described the procedure for implementing ship performance in brash ice in a square-type basin. They explain in detail the procedures to efficiently generate the brash ice channel, brash ice and resistance, and propulsion tests.

1.2. Experimental Advances

Guo et al. [21] conducted experimental tests with a container ship model in a towing tank with seven sizes of synthetic ice made out of paraffin wax. They intended to compare

the experimental results of the resistance in brash ice with the results of a numerical model based on the FE and FSI Methods. They carried out simulations that were validated against the experimental towing tank tests at different brash ice concentrations. Dobrodeev and Sazonov [22] proposed a method to estimate the ice resistance in a brash ice channel. They developed a mathematical model of ship motion in brash ice from full-scale and model test data. The total ice resistance was obtained as the sum of the resistance due to displacement of brash ice accumulations, momentum resistance, resistance due to friction of brash ice particles against the bow of the ship, stern and bottom and due to friction against sides of the ship. The model was validated through comparison with experimental data. Jeong and Kim [23] studied the features of ship resistance in pack ice conditions representative of the melting seasons. They carried out experiments in pack ice enclosed in a channel whose width, as well as the ice concentration and thickness, was varied for different tests, and found that the width of the channel is a key factor for obtaining accurate results in ice model testing. Van der Berg et al. [24] studied the influence of floe shape on the interaction of vertical-sided structures with broken ice. They concluded that the floe shape is important in clearance-dominated interactions and pointed out that the square floes typically used in the model tests experienced higher loads and resistance than those presented in real broken ice fields. This change in the results is due to larger networks of force chains in the broken ice around the structure. Zong et al. [25] conducted experiments to obtain ship resistance in small ice floes. These authors used artificial ice floes made of polypropylene (PP) with different distribution, floe size, and shape, according to field observations. They concluded that the floe shape has a slight influence in the resistance of the ship for low ice concentration and speed. Lastly, Van der Berg et al. [26] studied the repeatability of ice tank tests with broken ice. They used a four-legged structure and a ship hull model in their experiments, which were reproduced 20 times with numerical simulations based on the non-smooth discrete element method, from different initial positions. The authors concluded that test repeatability is poor in broken ice due to the features of this ice condition.

1.3. The Aim of This Work

With the aim of studying ship-block interaction and providing data for other research in which numerical tools will be developed, a wide number of tests were conducted at the CEHINAV towing tank (Madrid, Spain). This paper presents the obtained results, including the data for verifying and validating numerical simulations with solids at free surface, and the procedure developed to analyze ship-block interaction in a traditional towing tank with blocks made of paraffin wax. This artificial material makes it possible to work at room temperatures and provides a method to study such interactions. Photogrammetry was used to retrieve the initial position of blocks before each test. The paper is structured as follows. First, a view of the experimental facilities, ship model, and material used for simulating blocks is presented. Second, the main points of the experimental campaign are shown. Third, the obtained results from the tests are presented. Signal processing has been applied to find suitable comparisons. Then, discussions of the main findings of the experimental campaign are presented. Finally, conclusions about data and observations are shown.

2. Experimental Facilities

In this section, an overview of the experimental facilities, the selected ship model, and the artificial floes based on paraffin wax are shown. As pointed out above, the aim of this work is to provide valuable data for future numerical simulations of ship navigation under certain broken ice conditions, as well as to present the results of experimentation with paraffin wax artificial floes in order to investigate the influence of ship-block interaction on resistance.

2.1. Ship Model

The selected model is inspired by a research ship of the Spanish Army called B.I.O. Hespérides [27]. The hull has a compromise bow [13] valid for the navigation of the full-scale ship, that is, open drift ice or navigation with certain size of ice floes. Another motivation to select this vessel was the importance of this ship for Spanish polar research programs. The main characteristics of the full-scale ship and ship model are shown in Table 1. Figure 2a shows photograph of the model built for the tests and Figure 2b shows the hull body lines.

Table 1. Main parameters of full-scale ship and ship model selected for experimentation.

Parameter	Full Scale	Model
Length overall, LOA (m)	82.588	3.854
Waterline length, L_{wl} (m)	76.791	3.583
Breadth, B (m)	14.591	0.681
Depth, D (m)	12.102	0.565
Draught, T (m)	4.421	0.207
Full load displacement, Δ (t)	2725.86	0.277
Metacentric height, GM (m)	–	0.186
Pitch radii of gyration, R_{xx} (m)	–	0.821
Vertical distance to center of gravity from baseline, KG (m)	–	0.157
Longitudinal distance to center of gravity from Aft_{pp}, LCG (m)	34.867	1.627
Block coefficient, C_b (–)	0.542	0.542
Water plane coefficient, C_{wp} (–)	0.806	0.806
Mid-ship section coefficient, C_m (–)	0.863	0.863
Model scale, (–)	–	1:21.43

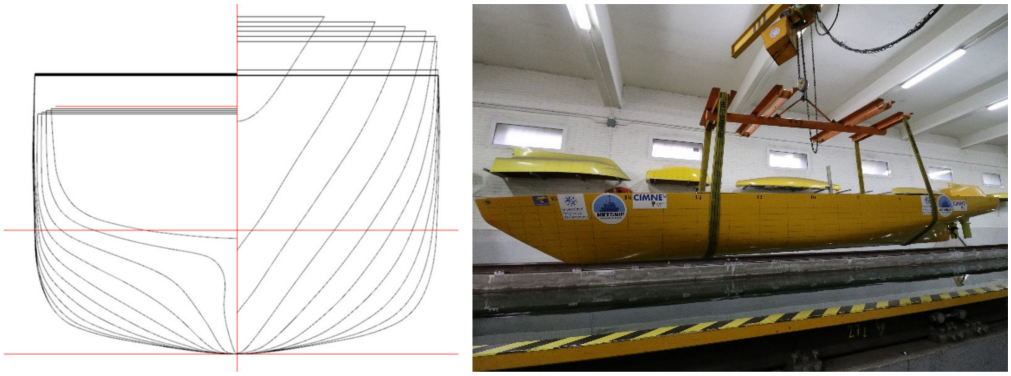

(**a**) (**b**)

Figure 2. (**a**) General view of the hull body lines of the ship model. (**b**) Photograph of the ship model built for experimentation.

The model dimensions are conditioned by the thickness of the blocks considered and the size of the available models of propeller established by the CEHINAV Research Group, applying a scale of 1:21.43.

2.2. Towing Tank Facilities

The tests were carried out in the model basin facilities of the Naval Architecture Department of Technical University of Madrid (Spain). A section of the basin was confined with metallic elements joined to the sides of the basin to simulate a floe-infested water zone and to take the measures for model-floe resistance. The main dimensions of the towing tank are 100 m of length, 3.8 m of width and 2.2 of draught. The dimensions of the artificial analysis section were 27 m of length and 3.8 m of width. The channel length was selected according to International Towing Tank Conference (ITTC) procedures and

similar works [18,21,28]. ITTC procedures recommend to allow the ship to proceed in level ice at least 1.5–2.0 times the ship length to obtain reliable values of resistance [29]. If the signal segmentation hypothesis is taken into account for future signal analyses, at least 10 segments of time series of resistance should be considered [29]. In our case, we decided to divide the signal into five segments and to increase the number of tests instead of enlarging the channel length, for practical purposes.

It should be noted that recommended practices are established for level ice [28], not for tests with ice floes. The floe section was large enough to allow the measurement of different parameters such as resistance and trim, among others. The tests simulated a ship navigating through an ice patch less than 27 m (term adopted for an area of floating ice less than 10 km across, the real scale being 578.61 m in this case [30]), a length barely seven lengths of the tested model, which is large enough to obtain appropriate results.

2.3. Paraffin Wax as Floes

Experimentation within the field of sea ice navigation often requires complex and expensive facilities, since suitable thermal conditions to conduct such tests are needed. ITTC also mentions the high cost and the time required for this type of experimentation in their recommended procedures [29]. New techniques are appearing to reduce the laboratory costs of this type of experimentation, boosted by the growing interest in polar technology. As mentioned in the introduction, some trends can be found related to artificial ice for experimental studies on the navigation of ships in the presence of ice floes.

An aqueous solution mixed with different chemical compounds can be used for simulating ice behavior (EG/AD/S mixture, as explained before). This compound has similar properties to sea ice, although it must be refrigerated. Other alternatives consist of using materials whose mechanical properties and density are similar to sea ice. Paraffin wax satisfies the requirement of density. In order to reproduce the desired friction effect on the hull, the friction coefficient must be provided according to the specific ice scenario and the scale of the prototype. Another proposal for a material to be used in experimentation could be polypropylene (PP). Examples of the use of PP can be found in [18,25].

For this work, paraffin wax was chosen because it has similar density to ice, since only floating blocks are considered and the breaking resistance is disregarded. A refined macro-crystalline paraffin wax type was used. This material could be a valid candidate to study the interaction between the ship and rigid bodies floating on the free surface resembling floes. Although obviously differences in behavior can be found between ice and paraffin, the use of the last material allows us to achieve the goals of this experimentation, that is, to provide data for future research in which a numerical framework will be developed to analyze the ship ice navigation, and study ship-floes resistance affordably. The main characteristics of paraffin wax are noted in Table 2.

Table 2. Main parameters of synthetic paraffin wax used as floe.

Parameter	Value	Units
Density	830	kg/m^3
Type	Macro-crystalline	(–)
Oil percentage (maximum)	0.5	%
Shape	Rectangular	(–)
Averaged thickness	40 mm	(–)
Friction coefficient hull-floe	0.25	(–)

Irrespective of the employed material, the movement of ice floes can be assumed to be rigid-body motion, since flexural or elastic deformation are negligible compared to the total body motion. In this research, no breaking resistance is considered. Similar hypotheses to ensure artificial floes do not suffer failures regarding bending stresses are assumed in [18,25].

3. Experimental Campaign

3.1. Block Distribution and Size

The size and the distribution of blocks throughout the channel constitute relevant parameters to be considered. There is scarce information about the distribution of floes in towing tank channels in the literature review. From observation in nature, different approaches can be achieved. Toyota et al. [31,32] works constitute a way to select a reasonable size of paraffin wax blocks according to real patterns of polar areas. These authors analyzed floe sizes and established expressions to determine the corresponding dimensions. According to their observations, we assumed scale invariance in fracture patterns of floes and considered a rectangular shape. The statistical properties of paraffin wax blocks are shown in Table 3. The number of fragments N_{ma} can be determined [32] as follows

$$N_{ma} = (1 - f)4f^m N_o \quad (1)$$

with f being a fragility coefficient, m the order of cell, and N_o the number of blocks with the largest size used.

Table 3. Statistics and fragility coefficient to determine the number of floes used in experimentation.

Parameter	Value	Unit
Fragility coefficient (f)	0.6	(–)
Mean thickness	40	mm
Percentage of the largest paraffin wax blocks	80	%
Mean length of the largest blocks	484	mm
Mean breath of the largest blocks	295	mm
Mean length of the smallest blocks	242	mm
Mean breath of the smallest blocks	148	mm

Different patterns are selected according to typical sea navigation [33] in broken ice, very open drift, and open drift ice. The corresponding concentrations of artificial floes on free surfaces are approximately equal to 30%, 45%, and 60%. It should be noted that typical sizes of ice floes in open drift ice fields are less than 20 meters in diameter [33]. The equivalent diameter of the full-scale ice path is 4.57 meters for the largest size according to our model scale (λ) equal to 1:21.43.

Two block sizes were selected for the tests. The former is the base size (the largest) with dimensions shown in Table 3, and the latter is one quarter of the largest block. The number of small blocks depends on the fragility coefficient f [31,32], taking exponent m equal to 1 from Equation (1). Only the largest type is employed with 30% concentration. For the rest of the concentrations, both sizes are considered. Depending on the area covered by blocks and the percentage of the largest blocks, different number of small pieces can be obtained.

The resulting size of blocks is nonsense if the thickness is constant in all blocks when the order for Equation (1) is high, i.e., m = 3 or 4. An example of this issue is shown in Figure 3, in which different orders of equations are considered. This expression should be used carefully if real distributions are analyzed. Larger sizes of blocks need to be considered if more than two sizes are introduced in the tests, assuming constant thickness.

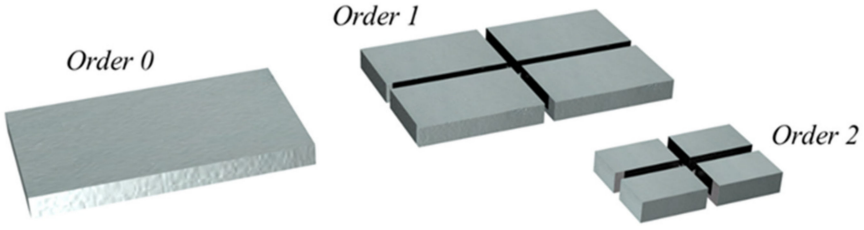

Figure 3. Block sizes according to different exponential orders of Equation (1).

Typical ice floe thickness ranges from 20 to 50 millimeters depending on the ship model scale for experimental tests in the literature. In our case, 40 mm is the thickness of floating blocks (see Table 3) according to the type of navigation of selected ship, as well as the ship classification (low polar class, ice thicknesses less than 1 meter). Table 4 shows the number of employed pieces for each concentration. Depending on the required concentration, different numbers of blocks according to Equation (1) are obtained.

Table 4. Number of blocks per coverage considered, and area covered in square meters.

Coverage (%)	Larger Size (Units)	Smaller Size (Units)	Area Covered (m^2)
30	207	–	29.6
45	251	240	44.4
60	447	429	79.1

Distributions on free surface of artificial blocks are in a random pattern, thus ensuring a homogeneous arrangement of all the space covered by paraffin wax blocks during the tests.

3.2. Capture System of Boundary Conditions in Initial Stationary State

The current development of numerical simulation code for studying the features of ship resistance in drift ice requires knowledge of the initial position of artificial ice floes before each test. To allow the obtained experimental results to serve as benchmark data for validating computational fluid mechanic code with floating objects on a free surface, an appropriate procedure has been conducted. In a literature survey, different examples of aerial views of test zones can be found, as in [25,26], for instance. Photogrammetry is a successful tool for capturing the initial boundary conditions of floes on a free surface. This technique is used in architecture and aerial surveillance. Photogrammetry is defined by the American Society for Photogrammetry and Remote Sensing (ASPRS) as "the art, science, and technology of obtaining reliable information about physical objects and the environment, through processes of recording, measuring, and interpreting imagery and digital representations of energy patterns derived from noncontact sensor systems" [34,35].

Terrestrial photogrammetry was used to obtain information regarding floes on the free surface of the towing tank. A commercial code was used to convert photos to useful information [36]. Then, the obtained information was processed to obtain a cloud of points (see hyperlink to Scipedia repository). Each block had two stickers separated a certain distance from each other to identify the type, the spin, and the location (see Figure 4a,b). The variables d, f represent the size of floes and α, the spin of the block.

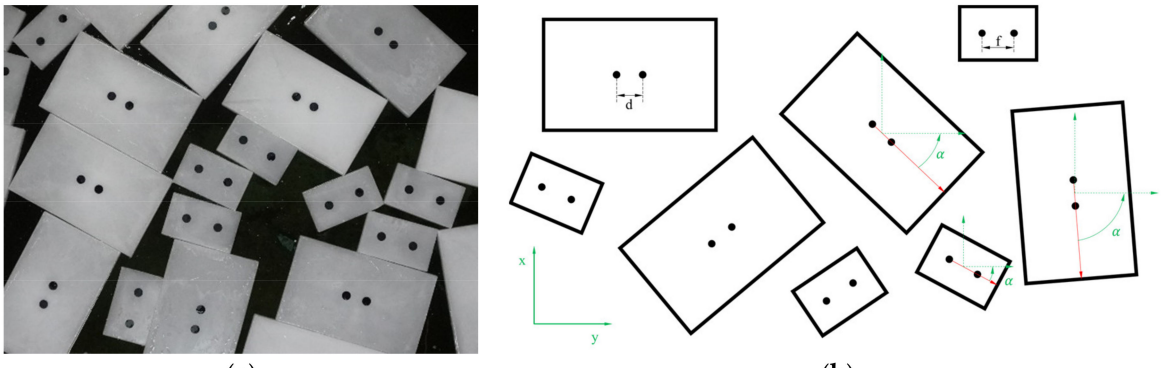

(**a**) (**b**)

Figure 4. (**a**) Photograph of floes on free surface. (**b**) Scheme of reference system adopted to determine the boundary conditions at the initial stationary state.

Keeping in mind the numerical data needed, the boundary conditions to be considered are: the space location in the global reference system, the spin of each block, and the size of the block. The adopted reference system takes the X-axis in the direction of the length of towing tank in a positive sense of carriage advance, and the Y-axis orthonormal to the last. Quick Response (QR) codes were placed at some points close to the free surface of the testing zone to give a reference for measuring data. Figure 5 shows a photograph of the carriage with the capture system.

Figure 5. Photograph of the carriage with capture system in the towing tank carriage.

The capture system was mounted on the carriage. Figure 6a,b show a scheme of the mounted capture system. It is formed by a frame, an extensible arm, and a camera system. The reference height of the cameras from the free surface is determined according to the focal length required to obtain an image capturing a certain area of free surface of the towing tank.

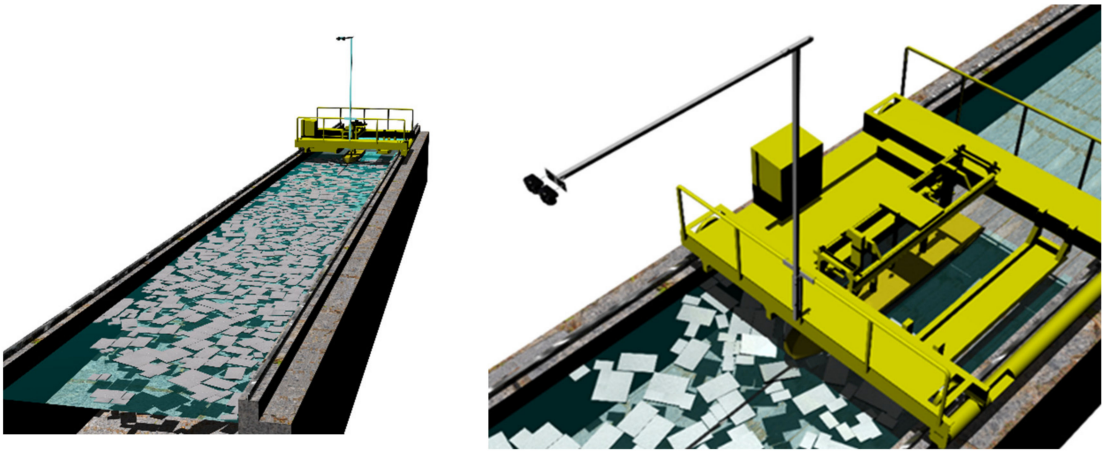

(**a**) (**b**)

Figure 6. (**a**) Details of the capture system mounted on the towing tank carriage. (**b**) General view of the towing tank. Right: detailed view of the carriage with capture system.

The ship model was disconnected from the carriage before each test. Then, the carriage ran along the testing zone. Next, the capture system recovered the information of the floes on the free surface. Finally, the ship model was connected again, and the run was performed. The information gathered was processed to obtain a map with a coverage pattern in each test.

Figure 7 shows an example of result obtained by the photogrammetry technique in the experimental campaign. A STereoLithography (STL) file was obtained when the shots were processed, and thus valuable information can be used to analyze the pattern distribution on the free surface. Figure 8a shows a combination of a photo with the STL file obtained from experimental campaign (see Figure 8b).

Figure 7. Example of STL file obtained for one test performed in experimental campaign.

(**a**) (**b**)

Figure 8. (**a**) Virtual model combined with shot obtained during experimental campaign. (**b**) Shot obtained during experimental campaign.

3.3. Tests

Three representative towing velocities were selected: 0.22 m/s, 0.33 m/s, and 0.53 m/s (corresponding with 2.0, 3.0, and 4.8 knots of the full-scale ship). In this way, the Froude numbers range from 0.037 to 0.090. As mentioned before, three free surface block distributions were managed. To reduce the uncertainty, five repetitions were conducted for

each type of test. The overall tests consisted of open water resistance tests and resistance tests with floes on free surface. After each run, the free surface coverage distribution was adjusted manually to obtain random patterns with homogeneous arrangements, as well as to avoid overlapping between blocks.

Bounds were mounted at the beginning and the end of the test zone (see Figure 9a,b). It is notable that bounds at the end of the channels caused blocks jams when the ship pushed blocks. This fact may cause problems in the reliability of the results, and therefore it is recommended to remove the bounds at the end to avoid this effect.

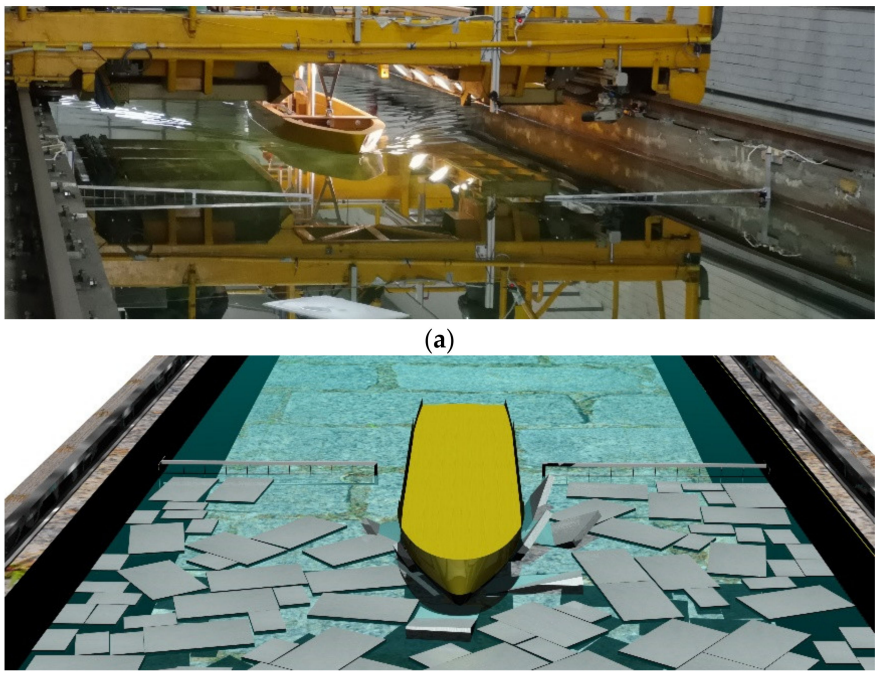

(**a**)

(**b**)

Figure 9. (**a**) Caption with bounds at the beginning of the test channel. (**b**) Model representation of the bounds at the beginning of the channel.

4. Results

The results from the tests were processed in order to give appropriate and valuable information about the experimentation. Raw data were managed in different ways. Firstly, statistic values of the time series for different tests were analyzed. Secondly, an uncertainty estimation of the randomness resistance was carried out. Figure 10 shows the curve of ship resistance for different Froude numbers.

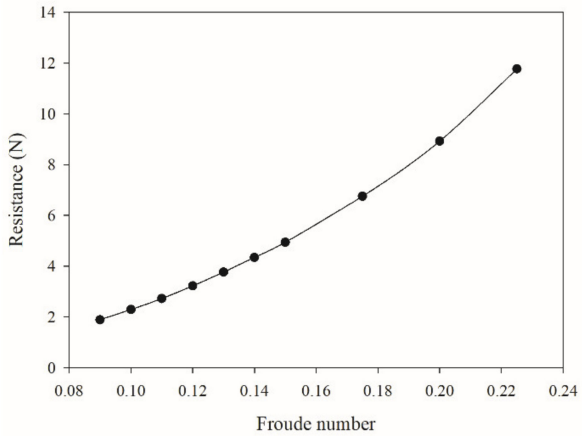

Figure 10. Open water resistance of ship model for different Froude numbers.

Tables 5–7 show the results for average, standard deviation, variance, and Root Mean Square (RMS) of each series of test carried out. Following ITTC procedures [28,29], segmentation of signal and the Chauvenet criterion were applied to remove outliers from raw data. From observations, no significative changes were found after applying the filter, although the values of average resistance were slightly lower (see Figure 11).

Table 5. Statistical values of total resistance obtained for Fr = 0.037. Average of each group of tests.

Coverage (%)	Average (N)	Standard Dev. (N)	Variance (N^2)	RMS (N)	Uncertainty (N)
30	2.746	7.335	62.510	7.884	0.983
45	5.394	7.080	52.316	8.924	0.952
60	10.174	11.547	134.396	15.445	0.791

Table 6. Statistical values of total resistance obtained for Fr = 0.056. Average of each group of tests.

Coverage (%)	Average (N)	Standard Dev. (N)	Variance (N^2)	RMS (N)	Uncertainty (N)
30	4.884	7.100	57.894	8.669	0.952
45	9.689	8.434	75.396	12.866	1.134
60	18.142	17.142	298.700	24.948	1.896

Table 7. Statistical values of total resistance obtained for Fr = 0.090. Average of each group of tests.

Coverage (%)	Average (N)	Standard Dev. (N)	Variance (N^2)	RMS (N)	Uncertainty (N)
30	6.551	5.962	36.736	0.902	1.734
45	14.396	14.141	212.725	20.221	2.303
60	21.927	23.732	420.834	27.243	2.707

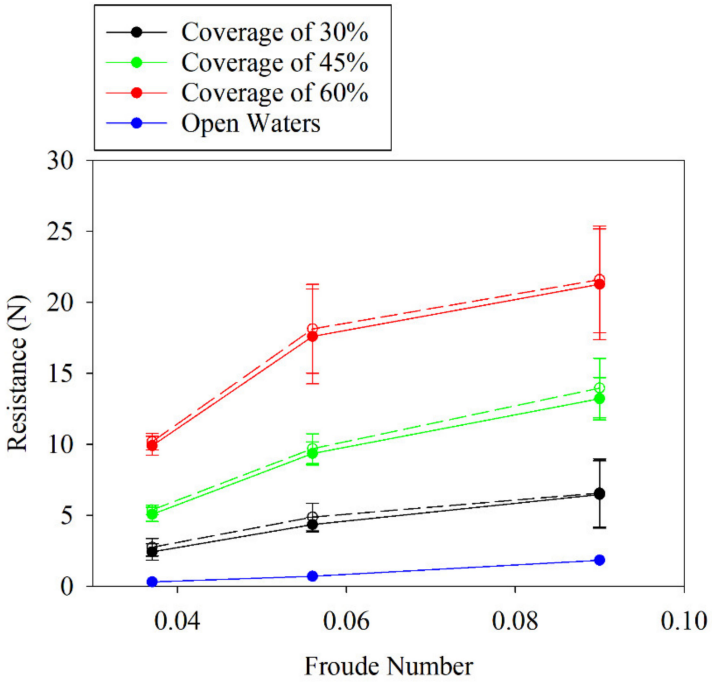

Figure 11. Comparison of resistance for different coverages and Froude numbers. Solid lines are the values applying the Chauvenet criterion. Dotted lines are the values without applying the Chauvenet criterion.

Each signal of raw data was processed, with smoothing of short-duration peaks of block impact load, and the signals were compared with each other. Figure 12 shows an example of the smoothing process applied to each signal.

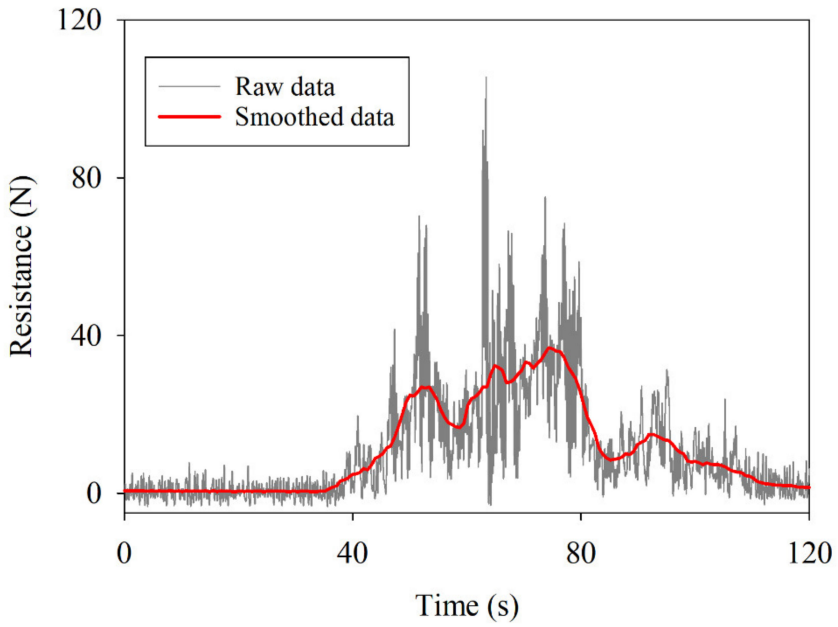

Figure 12. Time series of a resistance test. The black line is the raw data from one test. The red line is the smoothed curve obtained from a local smoothing technique that averages the values with neighborhood points.

The smoothing technique was also applied to each signal in order to obtain refined comparisons of data. Figures 13–15 show the smoothed time series for most tests. As can be noticed, similar average values are obtained. Peaks values can be observed in each run, showing variability in time series signals. The greater the coverage, the less the transitory variations in resistance, as can be deduced from the comparison in Figures 13–15, although this fact results in obtaining higher resistance, as expected. Each color line corresponds with a different run with the same velocity and coverage. In addition, it can be observed that resistance increases significantly as the Froude number increases. Peak values at the end of the time series at low coverage may be due to local accumulations of chains of blocks (similar phenomena have been observed in other research works, such as [24–26]).

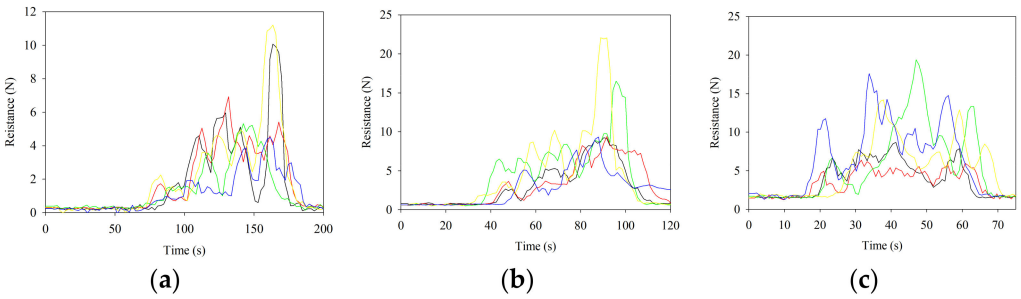

Figure 13. Smoothed time series of a resistance test for 30% coverage on free surface. Influence of Froude number: (**a**) Fr = 0.037; (**b**) Fr = 0.056; (**c**) Fr = 0.090. Different colors correspond with different tests carried out at the same velocity.

To obtain the statistics, significant values of resistance raw data within the testing zone were trimmed according to ITTC procedures for ice level navigation. Fourier analysis was applied to each trimmed time series, assuming a Gaussian data distribution. Then, through integration of a spectral signal, the significant values were obtained as follows for each run:

$$R_{sig} = 2\sigma = 2 \cdot \left(\int_0^\infty |R(\omega)|^2 \mathrm{d}\omega \right)^{\frac{1}{2}}, \quad (2)$$

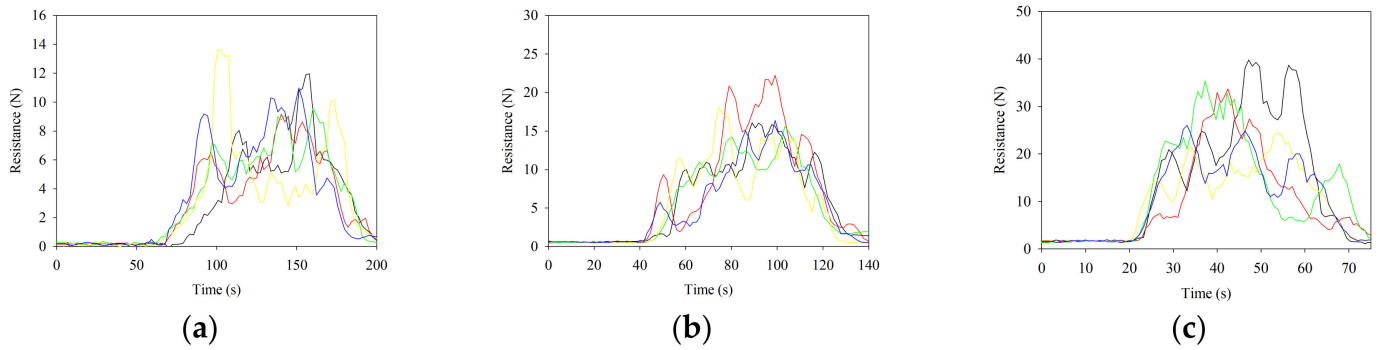

Figure 14. Smoothed time series of a resistance test for 45% coverage on free surface. Influence of Froude number: (**a**) Fr = 0.037; (**b**) Fr = 0.056; (**c**) Fr = 0.090. Different colors correspond with different tests carried out at the same velocity.

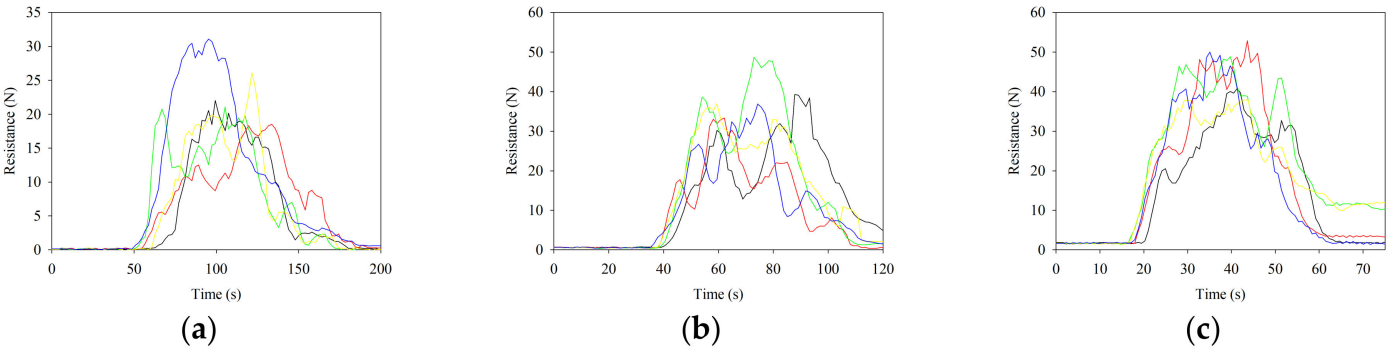

Figure 15. Smoothed time series of a resistance test for 60% coverage at free surface. Influence of Froude number: (**a**) Fr = 0.037; (**b**) Fr = 0.056; (**c**) Fr = 0.090. Different colors correspond with different tests carried out at the same velocity.

$R(\omega)$ being the resistance amplitude of each component of power spectral density, σ being standard deviation, and ω the angular frequency in rad/s.

Figure 16 shows the pitch angle during different runs at different coverages. It can be deduced that the more coverage, the more trim variation during the runs.

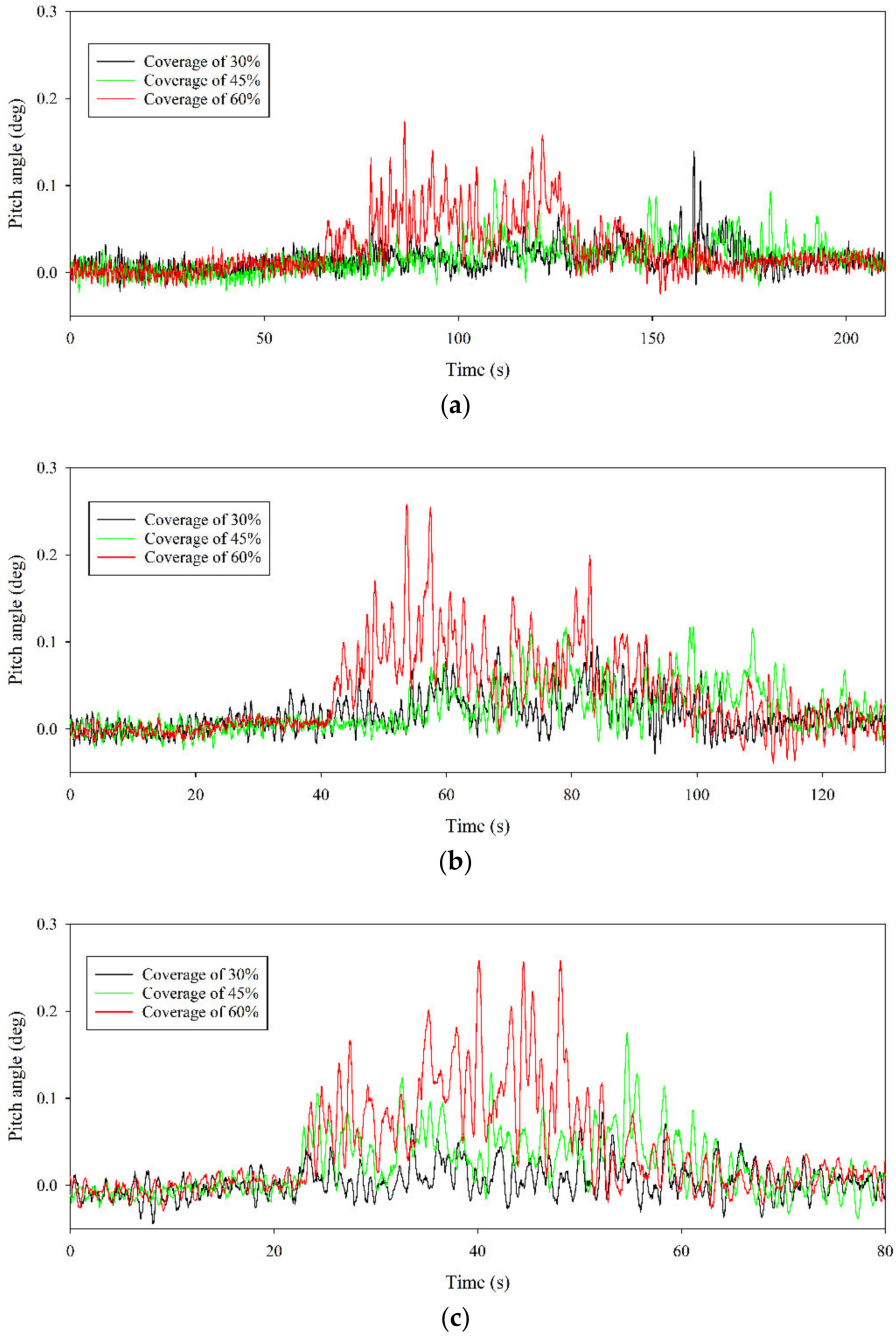

Figure 16. Pitch angle for different test velocities. (**a**) Fr = 0.037; (**b**) Fr = 0.056; (**c**) Fr = 0.090.

5. Discussion

The most relevant phenomena observed during the experimental campaign are discussed as follows. From the experimentation, changes in block concentrations on the free surface due to the ship advance were observed. In fact, accumulation processes due to ship-block interaction produced sizeable resistance changes. Similar observations have been made by other research works (see [24–26], for instance). Regarding blocks jams, the artificial bounds placed to ensure the enclosure of floes in the testing zone affected blocks concentrations at the end of the run. This type of phenomenon produces uncertainties in tests with artificial floes on a free surface.

5.1. Influence of Velocity and Concentration

Significant increases in ship resistance were detected in the experimental campaign when the blocks concentration increased (see Figure 11). Variations in ship resistance with velocity were more significant when block concentration increased from 30% to 45%, being double the increase from 45% to 60% concentration.

Ship resistance with floes was up to eight times higher than that for open waters. Similar increases have been reported in several works. For instance, Grochowalski and Hermanski, [13] reported larger variations between open waters and broken ice. Guo et al. [37] registered the same variations between open waters and navigation with floes at free surface. Analogous increments were obtained for 0.22 and 0.33 m/s velocities (Fr = 0.037 and 0.056 respectively). Nevertheless, greater differences, on order of twice those obtained for the velocity 0.33 m/s, were observed with the highest velocity 0.53 m/s (Fr = 0.09).

Analyzing Figures 13–15, it can be deduced that the evolution of resistance over time follows similar trends for all cases. Values of resistance were quite similar for same Froude number. The random distribution of blocks in each run introduced high differences in the signal retrieved. Comparisons show good agreement between each run and blocks distributions, especially with the largest concentration on free surface.

In the experimentation, the bow of the ship sometimes intercepted one or two blocks at the end of the run. This attachment effect produces larger deviations in mean resistance from those cases in which blocks are clearing (see Figure 17). This effect can be observed at the end of the time series in Figures 13–15. The same observations were noted by Zong et al. [25]. It is unclear if this phenomenon would occur in full-scale ship-ice interaction. Bending or splitting would be expected and therefore, the floe would fail in reality (see Supplementary Video S1).

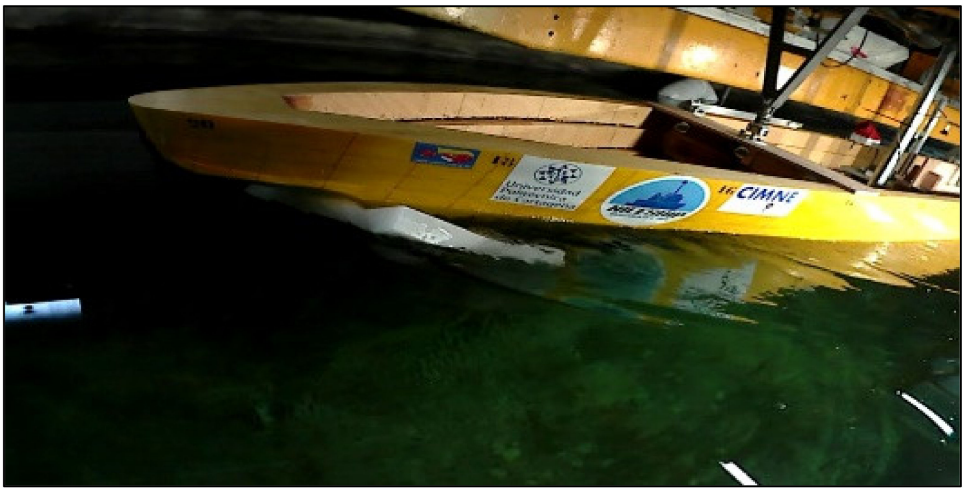

Figure 17. Attachment effect on ship bow.

Figure 18 shows the significant values obtained from the integration of spectral analysis of the trimmed signal time series versus coverage and velocity. No larger variations in significant values were found for low concentrations. This fact originates in the concentration itself. When the number of blocks on the free surface becomes lower, blocks have more space to move in the testing zone. Gaps between blocks are large enough to reduce the intensity of collisions, leading to a larger variation in signal. This can be explained by the fact that the bow of the ship can encounter some spaces with few floes and others with a high number of blocks, causing high differences for any Froude numbers under low coverage conditions during the same test. However, this effect cannot be observed when the concentrations are higher.

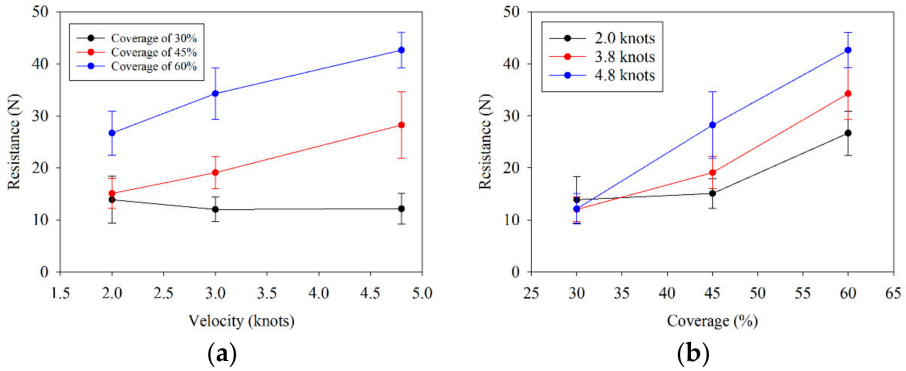

Figure 18. (**a**). Significant resistance value versus free surface coverage. (**b**). Significant resistance value versus velocity.

A practical comparison with different formulations was carried out to ensure that the results obtained are similar to those obtained with other formulations, and are also valid as a benchmark in numerical simulations. In spite of the stochastic nature of the problem, Figure 19 shows that resistance obtained from the experimentation has similar trends to those obtained with different formulations. For this comparison, Miko and Riska [38]'s formulation for brash ice and Zong and Zhou [39]'s, Aboulazm [40]'s, and Hung et al. [41]'s formulations for drift ice were used. In the case of brash ice, the comparison was carried out with results obtained with 60% coverage. Table 8 shows some of parameters required to conduct the comparison.

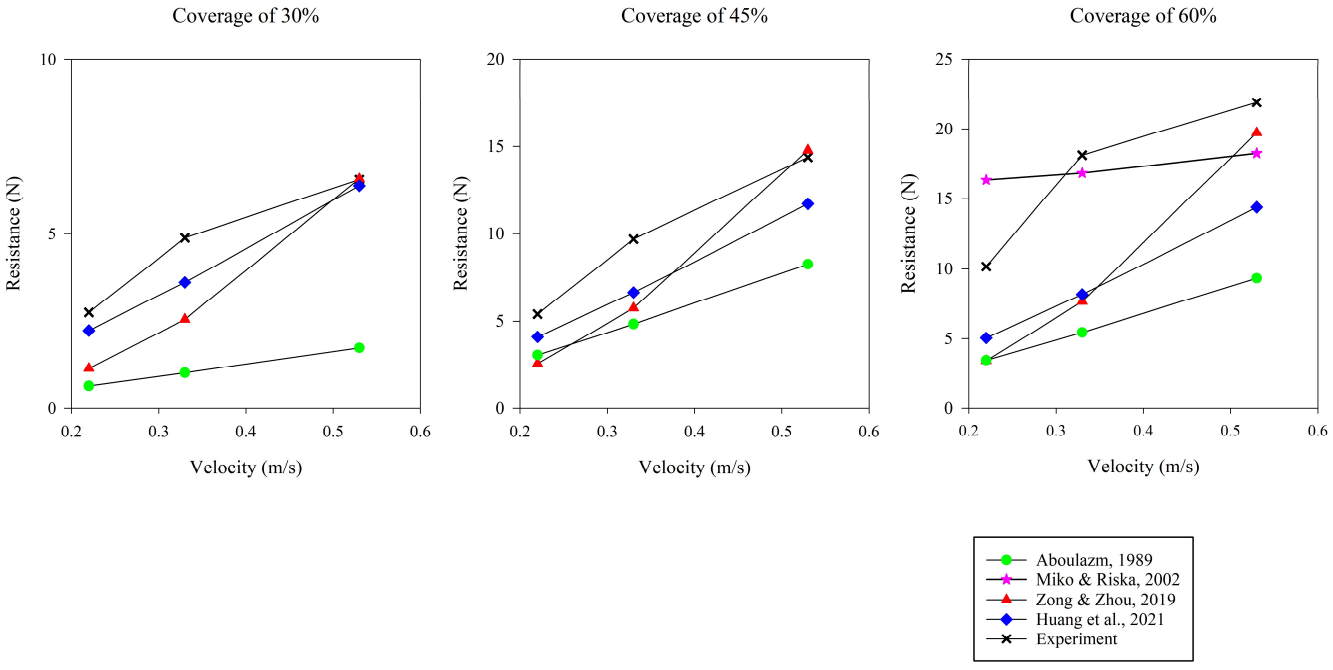

Figure 19. Comparison of different formulations with those averaged results obtained in experimentations with different coverages and Froude numbers.

Table 8. Parameters required to make comparisons with different formulations obtained from literature review.

Parameter	Value	Unit
Porosity, p	0.005	(–)
Constant of passive stress, K_p	0.5	(–)
Coefficient of lateral stress at rest, K_o	0.5	(–)
Length of parallel midbody at the waterline, L_{par}	41.3	m
Buttock angle, ϕ	66.7	deg
Waterplane entrance angle, α	20	deg
Waterplane area of foreship, A_{wp}	315	m^2
Slope angle and the sidewall, δ	22.6	deg
Added mass coefficient, C_a	1.6	(–)

As can be deduced from Figure 18, for a low concentration of 30%, similar trends to those of the analytical formulation were obtained. Higher differences were found for Fr = 0.056, and lower differences for Fr = 0.09. Aboulazm [40] predicted well for low Froude numbers, but differing by low values for the rest of the velocities. Zong and Zhou [39] and Hou et al. [41] obtained similar values for all Froude numbers through their formulations. A brash ice resistance comparison was introduced for 60% coverage. A low slope of brash ice resistance was found due to the low contribution of the quadratic term of velocity in the formulation [38]. In general, the resistance values obtained in the experimentation were in the order of those obtained by different formulations.

When the ship model enters the testing zone, the hull pushes blocks floating on the surface around the model waterline. Blocks push each other towards the wall of the towing tank, producing an interference effect leading to increased ship resistance. This increment in the measured resistance of the model needs to be further studied to determine ranges for the variables inducing this effect due to the channel width, such as model speed and dimensions, ice concentration, size of the ice floes, etc. Model tests for brash ice conditions require a channel width twice wider than the model's beam [8]. Pack ice conditions involve greater sizes of ice floes than brash ice conditions. Some researchers have investigated the effect of the width of channels in pack ice conditions at concentrations above 80s% and speed between 2–4 knots, concluding that it is recommended to have a channel width at least six [42] to eight [23] times wider than the model breadth to obtain accurate results. In our case, the channel width was six times wider than the model breadth.

Regarding the arrangement of blocks, it can be remarked that accumulations in front of the bow of the ship change the percentage of distribution in each test. Figure 20 shows a local accumulation with approximately a 70% of covered surface, in one of the experiments. Gaps between blocks are digitally colored in green. When the ship model advanced, wave propagation and the inertia effect of blocks generated forward movement of the floes. This effect was noticeable when the concentration of blocks increased (see Supplementary Video S2). Another relevant observation is the blocking effect produced by the boundaries at the end of the testing zone, if they are not removed.

5.2. Influence of the Size and the Shape of Blocks

Two sizes of rectangular paraffin wax blocks were used in the experimentations, as previously mentioned. The number of blocks with the largest size was 80% of the total in all cases. From comparisons of results obtained with different concentrations, it can be deduced that size has no apparent influence on mean resistance values.

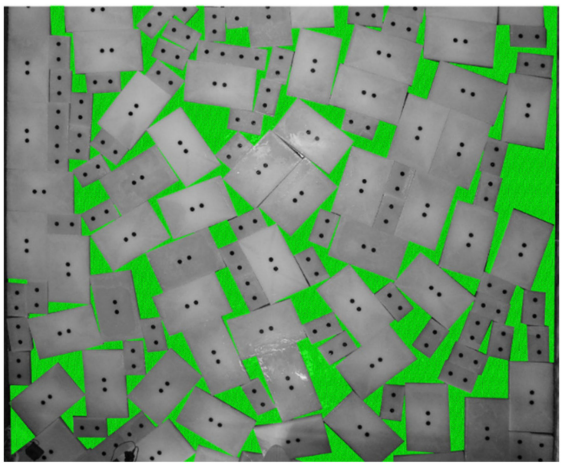

Figure 20. Example of local accumulation of blocks at the bow of the ship. Green color signifies the gaps between floes.

Observations during the tests can give a whole view of the phenomena occurred during testing. Sometimes, small size blocks helped the ship to reduce clearing resistance, since they permitted the largest blocks to slide against each other. This effect may have diminished the mean resistance in part of the testing zone.

The influence of the shape of the blocks was analyzed. For the experimentation, a rectangular shape is chosen, as aforementioned. It is necessary to recognize that this shape causes chains of blocks during tests (see Supplementary Video S3), as pointed out by several authors [23]. In general, these chains produce an increase of instant resistance and sometimes cause block jams. This influence can be neglected for the lowest concentration and velocity. Physically, the rectangular shape allows the blocks to stand next to each other, making block chains in which the connection between pieces is edge to edge at most times. Figure 21 shows an example of this phenomenon. The artificial floe chains extend more than one waterline length in some cases.

Figure 21. Example of chain block with 60% concentration on free surface.

5.3. Pattern Distribution for Different Tests

Keeping in mind that one key objective of this experimentation was to provide data to help other scientists and code developers to verify and validate numerical code with floating objects on free surface, it is mandatory to present experimental results related to values of mean resistance for the tests, as well as information about boundary conditions in

each run (see Supplementary Materials). The number of blocks on the free surface and the spatial location in a reference frame are relevant geometric information to provide.

As above explained, photogrammetry was used to obtain and identify the initial boundary conditions on the free surface. The positions of paraffin wax blocks were recognized through computational techniques. Figure 22 shows images corresponding to six distributions for 30%, 45%, and 60% (in the Supplementary Materials, the high-resolution images can be download from a Scipedia repository; see the hyperlink). Data with the initial positions of pieces are attached as well. Note that the patterns are essentially random for each distribution. Low concentrations sometimes obtain higher clearances between blocks, and therefore the bow of the ship may encounter open water and block fields alternatively. This fact introduced high oscillations in the signal retrieved. Although artificial material for floes is used in this work, it is reasonable to think that the nature of the navigation of a ship in water with broken ice could be similar to this type of pattern.

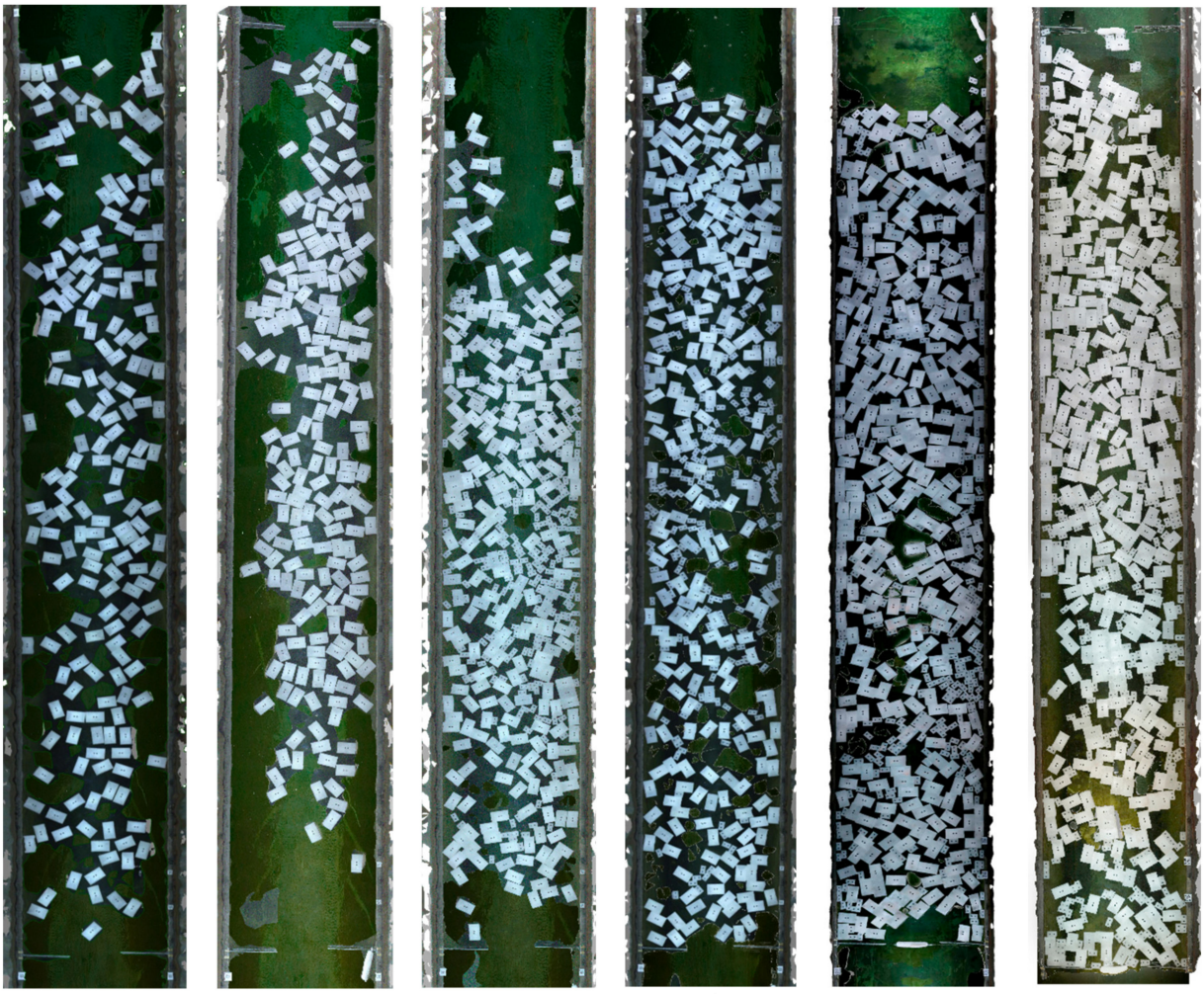

Figure 22. Distribution of coverages for different tests: (**a**,**b**) distributions for 30% of coverage; (**c**,**d**) distributions for 45% of coverage; (**e**,**f**) distribution of 60% of coverage.

It is clear that better repeatability of the test results may be achieved by using a regular pattern in broken block distribution on free surface, but this goal could be difficult to obtain due to the complex nature of the phenomena. Although downstream patterns in the field are similar in all tests, differences were found depending on the concentration and the velocity. Figure 23a,b show examples of downstream patterns for 30% and 60% of coverages, respectively.

(a) (b)

Figure 23. (**a**) Downstream distribution of blocks patterns at 30% coverage. (**b**) Downstream distribution of block patterns at 60% coverage.

Finally, note that in nature, ice floes have shapes more irregular that those considered in this work (mainly rectangular and forming block networks); therefore, it is expected that real resistance is minor compared to the presented results.

6. Conclusions and Further Research

Experimental campaigns were developed to investigate the interaction between floating blocks on a free surface and ship navigation. The main focus of the experimentation has been to analyze ship-block effects and provide valuable data to other scientists and code developers. From the observation carried out, some conclusions can be proposed:

- The use of paraffin wax could be an alternative to obtain affordable solutions to study ship-block interaction during ship navigation in broken ice conditions, avoiding the sometimes high cost of ice tests.
- Photogrammetry can be used to successfully determine the initial position of blocks before each test. The information retrieved can be used then to verify and validate numerical code with floating objects on a free surface. In our case, these data are provided as a service to other researches.
- It was observed that higher concentrations above 45% give a better quality of retrieved signal. Lower concentrations give higher oscillations compared with concentrations of 45% and 60%.
- The mean resistance may be influenced by the block shape. Edge to edge contacts were common in the observations made. Large chains of blocks were noticed mainly at high concentrations. It seems reasonable that the main resistance in real conditions could be less than that obtained from this experimentation. However, the main objective was to provide valuable data for other numerical developments to study ship navigation with objects on a free surface.
- Ship-block resistance reached up to eight times open water resistance. Many other works have obtained similar results, as aforementioned.
- Bounds at the end of the ice channel produce block jams. This phenomenon increases the instantaneous ship resistance.
- The attachment phenomenon in which the largest dimension of the block is perpendicular to the bow of the ship produces an increase in the ship resistance.
- The main findings explained above are based on measurements obtained from model tests under specific conditions. The information provided, together with the block distribution figures with different coverages, should help other researches.

Supplementary Materials: The following are available online at https://www.mdpi.com/article/10.3390/jmse10020246/s1: Video S1; Video S2; Video S3.

Author Contributions: J.E.G.-R., B.Z.-P. and S.R.-C., methodology; J.E.G.-R. and S.R.-C., software; J.E.G.-R., J.E.-P. and S.R.-C., validation; J.E.G.-R., B.Z.-P. and S.R.-C., formal analysis; J.P.L.-A. and J.E.G.-R., investigation; J.E.G.-R., B.Z.-P. and S.R.-C., writing—original draft preparation; J.E.G.-R., B.Z.-P., J.P.L.-A., J.E.-P. and S.R.-C., writing—review and editing; S.R.-C., visualization; J.E.G.-R., funding acquisition. All authors have read and agreed to the published version of the manuscript.

Funding: The research leading to these results has received funding from the Minister of Science and Innovation, State Research Agency, and the European Regional Development Fund under Grants RTI2018-094744-A-C22 (NICESHIP).

Institutional Review Board Statement: Not applicable.

Informed Consent Statement: Not applicable.

Data Availability Statement: All images and dataset are available at NICESHIP PROJECT: Scipedia. https://www.scipedia.com/public/Gutierrez_Romero_et_al_2021a (accessed on 1 March 2021).

Acknowledgments: The authors acknowledge CEHINAV, whose facilities made this work possible. Thanks to Juan-Luís Chacón, Luís Perez-Rojas, the CEHINAV research group, and the CIMNE naval research group for providing their knowledge and support to carry out this experimentation. Thanks to Carlos López-Pavón and Pablo Romero for providing their assistance during the experimentation.

Conflicts of Interest: The authors declare no conflict of interest.

References

1. Intergovernmental Panel on Climate Change (IPCC). *IPCC Special Report on the Ocean and Cryosphere in a Changing Climate*; Pörtner, H.-O., Roberts, D.C., Masson-Delmotte, V., Zhai, P., Tignor, M., Poloczanska, E., Mintenbeck, K., Alegría, A., Nicolai, M., Okem, A., et al., Eds.; IPCC: Geneva, Switzerland, 2019; *in press*.
2. Lasserre, F.; Beveridge, L.; Fournier, M.; Têtu, P.-H.; Huang, L. Polar seaways? Maritime transport in the Arctic: An analysis of shipowners' intentions II. *J. Transp. Geogr.* **2016**, *57*, 105–114. [CrossRef]
3. Timco, G.W. EG/AD/S: A new type of model ice for re-frigerated towing tanks. *Cold Reg. Sci. Technol.* **1986**, *12*, 175–195. [CrossRef]
4. Lau, M.; Wang, J.; Lee, C. Review of ice modelling methodology. In Proceedings of the 19th International Conference on Port and Ocean Engineering under Arctic Conditions (POAC'07), Dalian, China, 27–30 June 2007; pp. 250–362.
5. Lindqvist, G. A straightforward method for calculation of ice resistance of ships. In Proceedings of the 10th International Conference on Port and Ocean Engineering under Arctic Conditions (POAC'89), Lulea, Sweden, 12–16 June 1989; pp. 722–735.
6. Riska, K. *Performance of Merchant Vessels in Ice in the Baltic. Research Report/Winter Navigation Research Board, 52*; Helsinki University of Technology, Ship Laboratory: Helsinki, Finland, 1997.
7. Sandkvist, J. Conditions in Brash Ice-Covered Channels with Repeated Passages. In Proceedings of the 6th International Conference on Port and Ocean Engineering under Arctic Conditions (POAC'81), Quebec, QC, Canada, 27–31 July 1981; pp. 244–253.
8. Kitazawa, T.; Ettema, R. Resistance to ship-hull motion through brash ice. *Cold Reg. Sci. Technol.* **1985**, *10*, 219–234. [CrossRef]
9. Aboulazm, A.F. Repeated ice impacts and ship resistance in fragmented ice. In Proceedings of the 12th International Conference on Port and Ocean Engineering under Arctic Conditions (POAC'93), Hamburg, Germany, 17–20 August 1993; pp. 149–157.
10. Englund, K. The Need of Engine Power for Merchant Vessels in Brash Ice Channels in the Baltic. Master's Thesis, Helsinki University of Technology, Helsinki, Finland, 1996.
11. Wilhelmson, M. The Resistance of a Ship in a Brash Ice Channel. Master's Thesis, Helsinki University of Technology, Helsinki, Finland, 1996.
12. Molyneux, D. Estimating performance requirements for ships navigating to and from Voisey's bay. In Proceedings of the 18th International Conference on Port and Ocean Engineering under Arctic Conditions. (POAC'05), Potsdam, NY, USA, 26–30 June 2005; pp. 187–198.
13. Grochowalski, S.; Hermanski, G. Ship Resistance and Propulsion in Ice-Covered Waters: An Experimental Study. *Trans. Soc. Nav. Archit. Mar. Eng.* **2011**, *119*, 67–92.
14. Konno, A.; Saitoh, O.; Watanabe, Y. Numerical investigation of effect of channel conditions against ship resistance in brash ice channels. In Proceedings of the 21st International Conference on Port and Ocean Engineering under Arctic Conditions (POAC'11), Montréal, QC, Canada, 10–14 July 2011.
15. Konno, A.; Nakane, A.; Kanamori, S. Validation of Numerical Estimation of Brash Ice Channel Resistance with Model Test. In Proceedings of the 22nd International Conference on Port and Ocean Engineering under Arctic Conditions (POAC'13), Espoo, Finland, 9–13 June 2013.
16. Kim, M.-C.; Lee, S.-K.; Lee, W.-J.; Wang, J.-Y. Numerical and experimental investigation of the resistance performance of an icebreaking cargo vessel in pack ice conditions. *Int. J. Nav. Archit. Ocean Eng.* **2013**, *5*, 116–131. [CrossRef]

17. Kim, M.-C.; Lee, W.-J.; Shin, Y.-J. Comparative study on the resistance performance of an icebreaking cargo vessel according to the variation of waterline angles in pack ice conditions. *Int. J. Nav. Archit. Ocean Eng.* **2014**, *6*, 876–893. [CrossRef]
18. Van der Werff, S.; Brouwer, J.; Hagesteijn, G. Ship resistance validation using artificial ice. In Proceedings of the ASME 34th International Conference on Ocean, Offshore and Arctic Engineering (OMAE 2015), St. John's, NL, Canada, 31 May–5 June 2015.
19. Zhang, Q.; Skjetne, R.; Metrikin, I.; Løset, S. Image Processing for Ice Floe Analyses in Broken-ice Model Testing. *Cold Reg. Sci. Technol.* **2015**, *111*, 27–38. [CrossRef]
20. Jeong, S.-Y.; Jang, J.; Kang, K.-J.; Kim, H.-S. Implementation of ship performance test in brash ice channel. *Ocean Eng.* **2017**, *140*, 57–65. [CrossRef]
21. Guo, C.-Y.; Zhang, Z.-T.; Tian, T.-P.; Li, S.-Y.; Zhao, D.-G. Numerical Simulation on the Resistance Performance of Ice-Going Container Ship Under Brash Ice Conditions. *China Ocean Eng.* **2018**, *32*, 546–556. [CrossRef]
22. Dobrodeev, A.A.; Sazonov, K.E. Ice resistance calculation method for a ship sailing via brash ice channel. In Proceedings of the 25th International Conference on Port and Ocean Engineering under Arctic Conditions (POAC'19), Delft, The Netherlands, 9–13 June 2019.
23. Jeong, S.-Y.; Kim, H.-S. Study of Ship Resistance Characteristics in Pack Ice Fields. In Proceedings of the 25th International Conference on Port and Ocean Engineering under Arctic Conditions (POAC'19), Delft, The Netherlands, 9–13 June 2019.
24. Van den Berg, M.; Lubbad, R.; Løset, S. The effect of ice floe shape on the load experienced by vertical-sided structures interacting with a broken ice field. *Mar. Struct.* **2019**, *65*, 229–248. [CrossRef]
25. Zong, Z.; Yang, B.Y.; Sun, Z.; Zhang, G.Y. Experimental study of ship resistance in artificial ice floes. *Cold Reg. Sci. Technol.* **2020**, *176*, 103102. [CrossRef]
26. Van den Berg, M.; Lubbad, R.; Løset, S. Repeatability of ice-tank tests with broken ice. *Mar. Struct.* **2020**, *74*, 102827. [CrossRef]
27. CSIC. Unidad de Tecnología Marina. *Consejo Superior de Investigación Científica.* 2020. Available online: www.utm.csic.es (accessed on 10 February 2020).
28. ITTC. ITTC Recommended Procedures and Guidelines. Testing and Extrapolation Methods Ice Testing Resistance Test in Level Ice. In Proceedings of the International Towing Tank Conference, Venice, Italy, 8–14 September 2002.
29. ITTC. ITTC Recommended Procedures and Guidelines. Experimental Uncertainty Analysis for Ship Resistance in Ice Tank Testing. In Proceedings of the International Towing Tank Conference, Edinburgh, UK, 4–10 September 2005.
30. WMO. *Sea Ice Nomenclature. Volume 1—Terminology and Codes*; 5th Session of JCOMM Expert Team on Sea Ice; World Meteorological Organization: Geneva, Switzerland, 2014.
31. Toyota, T.; Takatsuji, S.; Nakayama, M. Characteristics of sea ice floe size distribution in the seasonal ice zone. *Geophys. Res. Lett.* **2006**, *33*, L02616. [CrossRef]
32. Toyota, T.; Haas, C.; Tamura, T. Size distribution and shape properties of relatively small sea-ice floes in the Antarctic marginal ice zone in late winter. *Deep Sea Res. Part II Top. Stud. Oceanogr.* **2011**, *58*, 1182–1193. [CrossRef]
33. CCG. *Ice Navigation in Canadian Waters*; Online; Canadian Coast Guard, Minister of Fisheries and Oceans: Ottawa, ON, Canada, 2012.
34. McGlone, C.; Mikhail, M.-E.; Bethel, J.-S.; Mullen, R. *Manual of Photogrammetry*; American Society for Photogrammetry and Remote Sensing: Bethesda, MD, USA, 2004.
35. Wolf, P.; Dewitt, B.; Wilkinson, B. *Elements of Photogrammetry with Applications in GIS*; McGraw-Hill: New York, NY, USA, 2014.
36. Bentley Engineering. *User Manual. ContextCapture; 3D Reality Modeling Software*; Online; Bentley: Exton, PA, USA, 2020.
37. Guo, C.-Y.; Xie, C.; Zhang, J.-Z.; Wang, S.; Zhao, D.G. Experimental Investigation of the Resistance Performance and Heave and Pitch Motions of Ice-Going Container Ship Under Pack Ice Conditions. *China Ocean Eng.* **2018**, *32*, 169–178. [CrossRef]
38. Miko, J.; Riska, K. *On the Power Requirements in the Finnish-Swedish Ice Class Rules*; Research Report no. 53; Ship Laboratory, Helsinki University of Technology: Espoo, Finland, 2002.
39. Zong, Z.; Zhou, L. A theoretical investigation of ship ice resistance in waters covered with ice floes. *Ocean Eng.* **2019**, *186*, 106114. [CrossRef]
40. Aboulazm, A.F. Ship Resistance in Ice Floe Covered Waters. Ph.D. Thesis, Memorial University of Newfoundland, St. John's, NL, Canada, 1989.
41. Huang, L.; Li, Z.; Ryan, C.; Ringsberg, J.W.; Pena, B.; Li, M.; Ding, L.; Thomas, G. Ship resistance when operating in floating ice floes: Derivation, validation, and application of an empirical equation. *Mar. Struct.* **2021**, *79*, 103057. [CrossRef]
42. Cho, S.-R.; Jeong, S.-Y.; Lee, S. Development of effective model test in pack ice conditions of square-type ice model basin. *Ocean Eng.* **2013**, *67*, 35–44. [CrossRef]